Title

Resolving the leftover problem for habitability and biosignatures on Enceladus

Supplementary Material

Author list

Antonin Affholder[a,b,c,1], Régis Ferrière[c,d,e], Sam Nasreldine[f] and François Guyot[g].

Affiliations

[a]Institute for Terrestrial Ecosystem Science, Department of Environmental System Science, ETH Zürich, Zürich, Switzerland. [b]Unit of Land Change Science, Swiss Federal Research Institute WSL, Birmensdorf, Switzerland. [c]Department of Ecology and Evolutionary Biology, University of Arizona, Tucson, Arizona, USA. [d]International Research Laboratory for Interdisciplinary Global Environmental Studies (iGLOBES), CNRS, ENS, PSL University, University of Arizona, Tucson AZ, USA. [e]Institut de Biologie de l'ENS, CNRS, INSERM, ENS, PSL University, Paris, France. [f]Program in Applied Mathematics, University of Arizona, Tucson, AZ, USA [g]Institut de Minéralogie, de Physique des Matériaux et de Cosmochimie Muséum National d'Histoire Naturelle, CNRS, Sorbonne Université, Paris, France

Contents

Supplementary Figures

Supplementary Tables

1 Supplementary text

1.1 Mechanistic foundation for the Michaelis-Menten equation

The Michaelis-Menten (MM) approximation for uptake is typically obtained by considering the steady-state flow of a resource R (substrate) to the interior of the cell. This flow is decomposed into two steps, whereas the resource molecule first has to encounter a transporter protein located at the cellular surface, and then the transporter actively imports the molecule into the cytoplasm[1–5]:

$$\mathrm{R} + \mathrm{E_f} \xrightarrow{k_1} \mathrm{X} \xrightarrow{k_2} \mathrm{R_I} + \mathrm{E_f} \tag{S1}$$

where $\mathrm{E_f}$ is a 'free' porter, X is the porter-substrate complex, and $\mathrm{R_I}$ is the internal substrate. While we illustrate here the derivation of the MM kinetics using the example of proteins transporting substrate to the cytoplasm ('porters'), this also applies to substrates that are processed at the cellular surface without importation to the cytoplasm (e.g. possibly dihydrogen). Note that equation (S1) assumes that the unbinding of substrate and porter is negligible, and that importation (step 2) is irreversible. Using the law of mass action, assuming steady-state for X ($\dot{\mathrm{X}} = 0$) and setting $[E] = [E_f] + [X]$, an equivalent to familiar MM equation is obtained:

$$U(S) = \dot{R}_I = k_2[\mathrm{E}]\frac{[R]}{[R] + \frac{k_2}{k_1}} \text{ mol s}^{-1} \tag{S2}$$

where $k_2[\mathrm{E}]$ ([E] counting the total number of mol of porter per cell) can be substituted for v_{max}, and k_2/k_1 for K_m. However, equation (S2) does not entirely represent how the uptake rate is a function of the density of transporters on the cellular surface. Indeed, [E] also determines the rate of encounter between porters and substrate k_1[6], such that the porter-specific rate of substrate capture k_1 in units of s^{-1} $(\mathrm{mol\ L}^{-1})^{-1}$ can be approximated by:

$$k_1 = \rho_w \mathscr{N}_A 4\pi D_w r_c \frac{r_p}{r_p[\mathrm{E}]\mathscr{N}_A + \pi r_c} \tag{S3}$$

where $\mathscr{N}_A = 6.022 \times 10^{23}$ mol^{-1} is Avogadro's number, $\rho_w = 1{,}000$ L m^{-3} converts m^3 to L, D_w (m^2 s^{-1}) is the diffusion coefficient of R in water, r_c (m) is the cell's radius (typically around 1 µm for Archaea), r_p is the radius of the porter protein assumed to be disk-like (typically taken to be 1 nm[6]), and [E] (mol) is the cellular porter density.

1.2 Gradient analysis of R^* under the MM-based model

Assuming Michaelis-Menten uptake, the limit resource value R^* follows (Box 1):

$$R^* = \frac{\gamma d K_m}{v_{max} - \gamma d} \tag{S4}$$

which is positive under the condition $v_{max} - \gamma d$ (in other words that there exists a positive value of R such that growth occurs faster than mortality). We now turn to the sensitivity of R^* to parameters assumed to change with temperature d, K_m, and v_{max}. To this end, we look at the first order Taylor expansion of a small relative increase of each parameter taken separately using:

$$\xi_i = \frac{x_i}{R^*} \frac{\partial R^*}{\partial x_i} \tag{S5}$$

where x_i is a variable among d, K_m, and v_{max}. By applying the expression in equation (S5) to equation (S4), we obtain:

$$\xi = \left(\xi_d = \frac{v_{max}}{v_{max} - \gamma d}, \xi_{K_m} = 1, \xi_{v_{max}} = -\frac{v_{max}}{v_{max} - \gamma d} \right) . \tag{S6}$$

Under the condition that $v_{max} > \gamma d > 0$, $v_{max}/(v_{max} - \gamma d) > 1$, implying that R^* is more sensitive to a relative increase in either v_{max} or d than in K_m. Interestingly, R^* is equally sensitive (with opposing signs) to a relative increase of d and to a relative decrease of v_{max}. Thus, if mortality and maximum uptake have the same sensitivity to temperature (for instance the same Q_{10}), R^* would change according to the sensitivity of K_m to temperature, which may be either positive or negative in principle (see Main Text), although mechanistic principles underlying K_m indicate that it should increase with temperature (see Main Text), in accordance with observation[7].

1.3 Activation energy of diffusion of H_2 in water

In order to approximate the activation energy for the diffusion constant of H_2 in water, we used the temperature data compiled in the CRC Handbook for Chemistry and Physics, Table 'Diffusion of Gases in Water'[8]. Using standard Arrhenius linear regression of $\ln D_w \propto 1/T$, we obtained ($R^2 > 0.99$, two-sided Wald test $p \approx 2 \times 10^{-8}$):

$$D_w^{H_2}(T) = (3.41 \times 10^{-6}) \times e^{-\frac{16{,}109}{RT}} \tag{S7}$$

i.e. that the diffusion constant of H_2 in water has an activation energy of 16.1 kJ mol^{-1} (Supplementary Figure S1).

1.4 Activation energy of v_{max}

Elias et al. (2014)[9] suggest that enzymes isolated from organisms adapted to various temperatures all have the same rate-temperature dependency, as captured by the empirical fold-increase of enzymatic rate per 10 K:

$$Q_{10} = \frac{k_{cat}(T+10)}{k_{cat}(T)} \tag{S8}$$

such that the temperature-rate scaling is approximated by:

$$k_{cat}(T) = k_{cat}(T_{ref}) Q_{10}^{\frac{T-T_{ref}}{10}} \tag{S9}$$

The existence of a universal Q_{10} implies that the activation energies of enzymes vary with the temperature at which organisms are adapted via

$$E_{a,c}(T_a) = RT_a \frac{T_a+10}{10} \ln Q_{10} \tag{S10}$$

where T_a represents the temperature at which the organism from which the enzyme is isolated is adapted. This suggests that the activation energy of a Arrhenius function representing the rate-temperature scaling of v_{max} should range from 45 kJ mol^{-1} at 273 K to 80 kJ mol^{-1} at 373 K, i.e. much higher than the activation energy for the diffusion constant for H_2 in water of 16 kJ mol^{-1}.

1.5 Analysis of the relation between R^* and T in the yield-limit model

Here, we analyze a generic version of the yield-limit model for any lithochemoautotrophic metabolism. Consider a generic catabolic reaction following the equation

$$-e_D + \sum_i Y_i R_i = 0 \tag{S11}$$

where R_i are all the reagents (reactants and products) of the catabolic reaction with the exception of the electron donor e_D and Y_i are the stoichiometric terms (negative for reactants and positive for products) which are normalized for 1 mole of electron donor (such that the stoichiometric coefficient of e_D is -1). Under the assumptions permitting to equate chemical activities with

concentrations, the Gibbs free energy per mole electron donor ($\mathrm{J\,mol^{-1}}$) for the catabolic reaction is given by:

$$\Delta_r G = \Delta_r G_0 + RT\left(\log \prod_i [R_i]^{Y_i} - \log[e_D]\right) = \Delta_r G_0 + RT \log Q' - RT \log[e_D] \tag{S12}$$

where we have defined $Q' := \prod_i [R_i]^{Y_i}$, brackets denote the concentration ($\mathrm{mol\,L^{-1}}$), $\Delta_r G^0$ is the standard Gibbs free energy of reaction, which is usually known for a given reaction, $R = 8.314$ $\mathrm{J\,K^{-1}\,mol^{-1}}$ is the ideal gas constant and T is the temperature in Kelvin units.

Recalling the expression for the steady-state Gibbs free energy of reaction for the yield model (Main Text equation (17)), neglecting the individual death rate unrelated to maintenance):

$$(-\Delta_r G)^* = \frac{e_m(T)}{q_{cat}(T)} \tag{S13}$$

we can solve for the electron donor concentration, yielding:

$$[e_D]^*(T) = Q' \times \exp\left[\frac{1}{RT}\left(\frac{e_m(T)}{q_{cat}(T)} + \Delta_r G_0\right)\right] \tag{S14}$$

where we recall that e_m is the biomass specific maintenance cost ($\mathrm{J\,mol^{-1}\,s^{-1}}$) and q_{cat} is the biomass-specific catabolic rate, or rate of electron donor processing ($\mathrm{s^{-1}}$). Differentiating equation (S14) with respect to temperature yields:

$$\frac{([e_D]^*)'}{[e_D]^*} = \frac{1}{RT}\frac{e_m(T)}{q_{cat}(T)}\left(\frac{e_m'(T)}{e_m(T)} - \frac{q_{cat}'(T)}{q_{cat}(T)} - \frac{1}{T}\frac{\Delta_r G_0 q_{cat}(T)}{e_m(T)}\right) . \tag{S15}$$

Whether the threshold $[e_D]^*$ increases with temperature is given by the sign of equation (S15). For catabolic reactions able to power the metabolism, it is often the case that $\Delta_r G_0 < 0$ (although it is not strictly required for the catabolic reaction to power metabolism in physiological conditions), in which case $e_m'/e_m > q_{cat}'/q_{cat}$ guarantees positivity of equation (S15). The points brought up in main text for $e_m'/e_m > q_{cat}'/q_{cat}$ stand here as the molecular basis for these rates is the same as v_{max} and d in the Michaelis-Menten based model. In the edge case that $\Delta_r G_0$ is slightly positive, the term in which it appears in equation (S15) should be vanishingly small, as the decomposition of the energy rate e_m should give a product between an energy term much greater than $\Delta_r G_0$ (E_m is of the order of a $\mathrm{MJ\,mol^{-1}}$ for autotrophs) and a biomass-specific rate term much larger than q_{cat}, owing to the scaling of the molecules which participate to metabolism and those which contribute to maintenance cost (essentially the entire cell; see ref.[10] for additional theoretical discussion). This ensures that even minute differences between

e'_m/e_m and q'_{cat}/q_{cat} imply that $[e_D]^*$ increases with temperature. These differences are likely not minute for microorganisms living at their preferred temperature, as the asymmetrical characteristic of the 'thermal growth curve' of microbes implies that the rate of maintenance/mortality increases much faster than metabolic rates at the optimal growth temperature.

1.6 Uncertainty in P-H_2 co-limitation curves

Co-limitation curves (see Box 2) are defined by:

$$\frac{1}{\gamma_{H_2}} U_{H_2}([H_2]_{cl}) = \frac{1}{\gamma_P} U_P([P]_{cl}) \tag{S16}$$

where the subscript *cl* denotes concentrations at which co-limitation occurs. In our study, we approximate uptake functions U_i using Michaelis-Menten kinetics:

$$U_i(R_i) = v^i_{max} \frac{R_i}{R_i + K^i_m} \ . \tag{S17}$$

Thus, equation (S16) rewrites

$$[P]_{cl} = K^P_m \frac{\Gamma([H_2]_{cl})}{1 - \Gamma([H_2]_{cl})} \tag{S18}$$

where

$$\Gamma([H_2]) = \frac{\gamma_P}{\gamma_{H_2}} \frac{v^{H_2}_{max}}{v^P_{max}} \frac{[H_2]}{[H_2] + K^{H_2}_m} \ . \tag{S19}$$

Whether the product

$$\lim_{[H_2]\to\infty} \Gamma([H_2]) = \frac{\gamma_P}{\gamma_{H_2}} \frac{v^{H_2}_{max}}{v^P_{max}} \tag{S20}$$

is greater or less than one qualitatively affects the shape of the co-limitation curve (equation (S16)). In essence, this captures whether H_2 or P limits growth when both are abundant (i.e. their concentration is much greater than their respective K_m values). Indeed, if equation (S20) is lower than one, then $[P]_{cl}$ should approach $K^P_m(1 + \lim_{[H_2]\to\infty}\Gamma)$ when H_2 becomes much greater than $K^{H_2}_m$, i.e growth tends to be limited by H_2 in ideal conditions. However, if $\lim\Gamma > 1$, then there exists a value of $[H_2]$ for which equation (S18) becomes indefinite ($\Gamma = 1$), i.e. growth tends to be P-limited in ideal conditions. In our three parameterizations, it is the latter which is occurring, i.e. methanogens should be P-limited rather than H_2-limited when both are abundant. However, our empirical ranges for $v^{H_2}_{max}$, v^P_{max}, γ_{H_2} and γ_P could in principle allow for combinations in which $\Gamma_\infty > 1$. Hence, that our three parameterizations have Γ_∞ rests on the particular selection of cases for the kinetic parameters for each resource, although

assuming that they would be correlated is not without merit (see Main text). In sum, we argue that we should typically expect hydrogenotrophic methanogens to be P rather than H_2 limited when both are abundant, but only empirical measurements of the uptake machinery for both resource in the same strain may resolve this. Speculatively, this should be expected to vary between strains and the environment from which they are isolated, as this behavior may be a by-product of adaptation of uptake machinery to conditions that typically differ widely from overabundance of every resource. As a note, such a difference between qualitative properties in the 2-resource system does not exist for the determination of the lines separating the basin in which trajectories reach the H_2 threshold (but not the P threshold) from the basin in which the opposite occurs.

1.7 Monte-Carlo Markov Chain sampling of initial conditions that best predict plume composition as final state

General approach To identify concentrations which when used as initial conditions of our 2-resource-1-population model (Main Text equations (11)) yield final, biotic, steady-states that best match the ranges of concentrations of H_2 and P inferred from chemical analysis of Enceladus's plume, we perform a Monte-Carlo Markov Chain (MCMC) sampling using Metropolis's algorithm. To do so, we first define the target distribution used to measure the likelihood of model outputs. This distribution is assumed to 2-dimensional log-normal, centered on the log-average of the ranges of assumed H_2 and P concentrations in the source material for the plume. In this case, we use the upper bound for the H_2 range ($1 \times 10^{-2}\,\mathrm{mol\,kg^{-1}}$) as estimated in Glein and Truong (2025)[11], and we take as lower bound the estimate by Waite et al. (2017)[12] ($2 \times 10^{-7}\,\mathrm{mol\,kg^{-1}}$) for a log-average value of $\approx 4.5 \times 10^{-5}\,\mathrm{mol\,kg^{-1}}$. For P, our log-average is $4.1 \times 10^{-3}\,\mathrm{mol\,kg^{-1}}$. Then, we assume this multivariate log-normal distribution to have a diagonal covariance matrix where the diagonal elements are set such that the span (in log scale) of the ranges identified in Main Text Methods section *H_2 and P concentration ranges* captures 99% of the distribution's spread (as if the ranges corresponded to 3σ error bars). This allows us to numerically evaluate the target probability density function, noted f_t, of proposed simulation final states $([H_2]_\infty, [P]_\infty)$ using SciPy[13].

Model implementation To simulate biotic steady-states as a function of boundary initial abiotic conditions, we first identify the minimal H_2 and P minimally viable concentration thresholds according to Main Text equation (9; Box 2) where the uptake function chosen to

be Michaelis-Menten:

$$\begin{cases} [\mathrm{H_2}]^* = \dfrac{\gamma_\mathrm{H} d K_\mathrm{H}}{v^\mathrm{H}_{max} - \gamma_\mathrm{H} d} & \text{(S21a)} \\ [\mathrm{P}]^* = \dfrac{\gamma_\mathrm{P} d K_\mathrm{P}}{v^\mathrm{P}_{max} - \gamma_\mathrm{P} d} & \text{(S21b)} \end{cases}$$

using our smoothed approximation of parameter values (*Supplementary text*), where parameters d, $\gamma_{\mathrm{H_2}}$, γ_P, $K_m^{\mathrm{H_2}}$, K_m^P are function of temperature (see *Construction of cases* in Main text Methods). In doing so, we smoothly explore the range of resource thresholds between the minimum ($[\mathrm{H_2}]^* = 2.75 \times 10^{-9}\,\mathrm{mol\,L^{-1}}$ and $[\mathrm{P}]^* = 2.81 \times 10^{-11}\,\mathrm{mol\,L^{-1}}$) and maximum ($[\mathrm{H_2}]^* = 5.6 \times 10^{-6}\,\mathrm{mol\,L^{-1}}$ and $[\mathrm{P}]^* = 2.71 \times 10^{-8}\,\mathrm{mol\,L^{-1}}$) in our parameterizations (Supplementary Table S1).

Then, given proposed boundary abiotic initial conditions $[\mathrm{H}]_0$, $[\mathrm{P}]_0$ and temperature T, we first check whether they are viable ($[\mathrm{H_2}]_0 > [\mathrm{H_2}]^*$ and $[\mathrm{P}]_0 > [\mathrm{H}]^*$) and then identify the steady-state limiting resource which is $\mathrm{H_2}$ if

$$[\mathrm{P}]_0 > [\mathrm{H_2}]_0 \frac{\gamma_P}{\gamma_H} + [\mathrm{P}]^* \quad \text{(S22)}$$

or P otherwise. Then, the steady-state concentration of the non-limiting resource is set by (see Box 2):

$$[R_n]_\infty = [R_n]_0 - \frac{\gamma_n}{\gamma_l}([R_l]_0 - [R_l]^*)\ . \quad \text{(S23)}$$

This formally results in a numerical procedure to evaluate the function $\pi : ([\mathrm{H_2}]_0, [\mathrm{P}]_0, T) \mapsto ([\mathrm{H_2}]_\infty, [\mathrm{P}]_\infty)$.

Monte Carlo Markov Chain sampling We now use the model π, and the target probability density function f_t (defined by the plume observations) to feed into a Metropolis algorithm with a multivariate normal proposal distribution (log-scaled for $[\mathrm{H_2}]_0, [\mathrm{P}]_0$, linear for T) with standard deviations of 0.01, 0.01 and 3 respectively. We define our acceptance ratio as $f_t(\pi(\mathbf{x_p}))/f_t(\pi(\mathbf{x_t}))$ where $\mathbf{x}_t$ is the current state $([\mathrm{H_2}]_0, [\mathrm{P}]_0, T)$ and $\mathbf{x}_p$ the proposed state. We allow for a burn in period of 50,000 steps, then run the MCMC algorithm until 150,000 samples of initial conditions have been accepted.

Plume best match hydrothermal $\mathrm{H_2}$ for hydrogenotrophic methanogenesis Affholder et al. (2021)[14] describe a model of mixing of ocean water and hydrothermal fluid designed to simulate hydrothermal methanogens at Enceladus's seafloor. This model of mixing calculates the overall output of the hydrothermal environment as fluxes of $\mathrm{H_2}$ and $\mathrm{CH_4}$ being released to the ocean as a upward-rising plume. Affholder et al. (2022)[14] simulate values of these fluxes under various conditions of hydrothermal fluid and ocean temperatures and compositions

(concentrations of CO_2, CH_4, and H_2), as well as by including or not the feedback of hydrogenotrophic methanogens on their local environment of the mixing layer at the core-ocean interface. Then, under the assumption that the bulk concentration of H_2 and CH_4 in Enceladus's ocean are at steady-state, these fluxes are compared with the escape fluxes of H_2 and CH_4 in Enceladus's space plume as constrained by measurements carried out by the Cassini mission[12]. Affholder et al. (2022)[15] then construct a 'posterior' set of biotic simulations, by retaining the 500 simulations closest (by euclidean distance in the H_2 and CH_4 escape fluxes space) to Cassini observations[12]. By doing so, they identified the set of parameters (hydrothermal fluid and ocean temperature and concentrations of H_2, CO_2, and CH_4) that yield the simulations that best match plume observables when methanogens are included in the model. By fitting a gaussian curve to the values of H_2 concentrations in the hydrothermal fluid used in the simulations that make up the 'posterior' set, a 95% interval of the 'posterior' H_2 concentration in the hydrothermal fluid is obtained (section 2.5 of ref.[15]). This interval is 100-600 $\mathrm{mmol\,L^{-1}}$. Of important note, this concentration is that of the hydrothermal fluid used in the simulations of ref.[14], however, in those simulations methanogens may locally experience any concentration between that of the hydrothermal fluid and that of the ocean, as they simulate a radial gradient. The ocean concentration in ref.[14] is taken to be lower than that of the hydrothermal fluid, thus, the 'posterior' range used here corresponds to the higher upper limit of the concentration that methanogens would experience locally at the seafloor, and does not correspond to that of the bulk of the ocean.

1.8 Global feedback of hydrothermal, energy-limited, methanogens on P budget in the bulk ocean

An upper limit to biomass productivity of energy-limited hypothetical methanogens at Enceladus's seafloor consistent with methane emission flux in the space plume is $1 \times 10^6\,\mathrm{kg_C\,yr^{-1}}$ [15,16]. By multiplying this estimate by the biomass-specific demand of P for methanogens (γ_P), a total P-demand by this hypothetical population of methanogens can be obtained. An upper estimate for γ_P is $\approx 0.71\,\mathrm{mmol_P\,g_{dw}{}^{-1}}$ (Methods). Assuming that roughly half of a cell's dry weight is carbon[17], the total demand of P by Earth-like methanogens at Enceladus's seafloor would be on the order of $1 \times 10^5\,\mathrm{mol_P\,yr^{-1}}$. Scaled to the mass of Enceladus's ocean (on the order of 1×10^{19} kg [18]), this would result in a globally averaged consumption rate of the order of $10\,\mathrm{nmol_P\,L^{-1}\,Myr^{-1}}$. Geochemical calculations constrain bio-available P at concentrations exceeding $100\,\mathrm{nmol\,L^{-1}}$ [19,20]. Thus, methanogens could in principle exhaust the oceanic P

budget in as little time as 10 Myr. Geochemical calculations assume dissolution equilibrium, implying that depletion of dissolved P may allow more mineral P in the core to be dissolved. Most importantly, such a low concentration of P disagrees with analysis of plume composition[21], which instead indicates concentrations of bio-available P in the ocean in excess of 1 mmol L^{-1}, consistent with dissolution of a large fraction of P present in the core of chondritic composition[19]. Under this scenario, biotic consumption could be sustained for several billion years without noticeable impact on the concentration of P in the bulk ocean.

1.9 Other bio-essential elements

The availability of bio-essential nutrients other than P could constrain Enceladus's habitability or limit the growth of putative organisms. Nitrogen is expected to be abundant in Enceladus's ocean[12], and recent findings support that Fe and S are also likely relatively abundant[22]. Deriving the growth thresholds for these elements requires that specific uptake parameters be estimated. However, knowledge of the order of magnitude for the biomass yields relative to these elements is sufficient to constrain whether biotic consumption may be commensurate with their estimated availability in Enceladus's ocean. As an approximation, it can be observed that at concentrations much greater than thresholds, the line in the 2-resource space that delimits trajectories that go to either one of two resource being limiting at biotic steady-state (equation 10 in Box 2 in Main text) becomes approximately one of line γ_2/γ_1 with intersect 0.

Interconversion of organic nitrogen and ammonia does not require the nitrogen atom to change oxidation state. Ammonia/ammonium can be used by microbes to assimilate nitrogen into biomass, and is returned by the degradation (including the fermentation) of N-containing organic matter, such as proteins. In anaerobic conditions, this would in principle constitute a simplified nitrogen cycle[23]. For the sake of sanity-checking the assumption that this cycling could keep methanogens in N-replete conditions, we roughly calculate the N demand implied by H_2-limited primary production plausible for Enceladus's seafloor and compare this to the dissolved ammonium/ammonia stock implied by ammonia found in the plume[12]. Cleveland et al., 2007 [24] show the elemental ratio C:N:P (60:7:1) of soil microbial biomass to be globally constrained. The Redfield ratio suggests elemental ratios C:N:P closer to 106:16:1 in planktonic biomass. In the first order, this indicates that methanogens are expected to require between 1/7 and 1/16 moles of N per mole of carbon that they fix. Replicating the same approach as in the previous, section, this indicates that a plausible nitrogen demand, scaled to ocean mass, for a population of H_2-limited methanogens at Enceladus's seafloor be approximately 0.5

to $1.2\,\mathrm{nmol\,L^{-1}\,kyr^{-1}}$ (see Table 1. in ref.[25] for the range of total ammonia concentration assumed here). A credible range for ammonium/ammonia in Enceladus's ocean can be as low as in the order of $10\,\mathrm{nmol\,L^{-1}}$ and up to $\approx 1\,\mathrm{mmol\,L^{-1}}$, indicating that N-cycling in Enceladus's seafloor would be required to turn nitrogen over on the 10,000 years timescale at the fastest, longer than typical the typical timescale of biomass degradation. Thus, it does not appear an implausible assumption that nitrogen cycling would sustain available nitrogen at non-limiting concentrations. Second, at $[\mathrm{N}] >> [\mathrm{N}]^*$, the line which separates H_2-limited steady-state from N-limited steady states is $[\mathrm{N}] \approx (1/400) * [\mathrm{H_2}]$ (taking $\gamma_{\mathrm{N}} \approx 1/10$ molN per molC and $\gamma_{\mathrm{H_2}} \approx 40$ molH_2 per molC). This means that as an approximation, most of the plausible abiotic ranges for H_2 concentration and for N concentration satisfy $[\mathrm{N}] \geq (1/400) * [\mathrm{H_2}]$. In sum, N does not seem to be a good candidate element for long term limitation of biomass production on the long term in Enceladus's ocean, and while H_2-limited biotic steady-state appears more plausible than N-limited biotic steady-state, the latter cannot be entirely ruled out.

Xu et al., (2025) [22] show that iron (Fe) and sulfur (S) can be expected to be found at concentrations in excess of $[\mathrm{Fe}] > 1 \times 10^{-8}\,\mathrm{mol\,L^{-1}}$, $[\mathrm{S}] > 1 \times 10^{-6}\,\mathrm{mol\,L^{-1}}$. Both sulfur or iron, depending on their oxidation state can be electron donor or acceptors of various metabolisms, but we ignore this case here to focus on whether these elements could be sufficiently abundant to be assimilated into the biomass of an ecosystem assumed to have methanogenesis as its primary production performing metabolism. Xu et al. (2025) [22], compiled that the iron quota in phytoplankton is in the order of 10^{-4} mol per molC or below, and the sulfur one is smaller than 3×10^{-2} mol per molC. Using the same approximation as above indicates that even at the upper range for plausible abiotic H_2 concentration from Glein and Truong (2025) [11], around $10\,\mathrm{mmol\,L^{-1}}$, and assuming the upper limit for cellular quotas, the concentration of Fe needs to be greater than $2.5 \times 10^{-8}\,\mathrm{mol\,L^{-1}}$ and that of S greater than $7.5 \times 10^{-6}\,\mathrm{mol\,L^{-1}}$. At the highest, H_2-limited methanogens at Enceladus's seafloor would have a globally averaged assimilation rate of S of $0.25\,\mathrm{\mu mol\,L^{-1}\,Myr^{-1}}$, and a assimilation rate of Fe of $0.8\,\mathrm{nmol\,L^{-1}\,Myr^{-1}}$. Thus, limitation of growth by Fe or S is unlikely to occur for methanogens at Enceladus's seafloor.

With sulfur, nitrogen, and phosphorus (and carbon and hydrogen), all major constituents known biomass have been reviewed here. However, other minor elements could be proposed as limiting factors for the growth of hypothetical methanogens in Enceladus's ocean. It is impossible, and pointless, to consider all possible limiting elements, as the composition of hypothetical alien life in Enceladus's ocean is unknown. However, it is interesting to briefly consider what minor elements are typically found in the metabolic enzymes of Earth's methanogens to propose

elements, the discovery of which in Enceladus's samples would comfort the hypothesis of the subsurface ocean being habitable to Earth-like methanogens. All known methanogens rely on ferredoxins, that is iron-sulfur proteins, for electron transfer steps of their metabolism. Because both iron and sulfur are expected in Enceladus's ocean, this should not pose an important additional constraint to our analysis above where the fraction of iron and sulfur in the bulk biomass is considered. Methanogenic archaea are also known to depend on the availability of nickel (Ni), and to a lesser extant on the availability of cobalt (Co) and molybdenum (Mo), for their growth[26]. Nickel is used in several of the key enzymes of methanogenic metabolisms, but may occasionally substituted for iron[27]. Ref.[26] have found that these metals no longer affect the growth of *M. thermoautotrophicum* when their concentration is greater than $\approx 100\,\mathrm{nmol\,L^{-1}}$. Can these metals be expected to be available at concentrations $> 100\,\mathrm{nmol\,L^{-1}}$ in Enceladus's ocean? This depends primarily on the bulk composition of Enceladus's accretion materials and on whether these elements can be transferred to the ocean compartment at sufficient efficiency. Comets and chondrites have been suggested as having compositions analog to the accretion material of outer solar system bodies[28], and silica nanograins found in Enceladus's plume have been suggested as evidence of hydrothermal alteration of a chondrite-like rocky core[29]. Ryugu samples were found to contain nickel, cobalt and molybdenum at appreciable levels[30], and Bennu samples contain nickel and cobalt[31]. Moreover, Fisher and Ferrière (2026) [32] suggest the viability of the methanogenic metabolic network supported by elements present in asteroid and meteorites. Bulk abundance of cobalt, nickel and molybdenum in Ryugu samples suggest that if Enceladus's was accreted from similar materials, nickel and cobalt could be present in the ocean at concentrations greater than $100\,\mathrm{nmol\,L^{-1}}$, and moolybdenum at a concentration greater than $10\,\mathrm{nmol\,L^{-1}}$, if entirely transferred to the ocean. The actual composition of Enceladus's accretionary material remains unknown, and the potential for these metals to leech into Enceladus's ocean is beyond the scope of this paper. Any hydrothermal setting at Enceladus's seafloor would likely be a hot spot for past or ongoing release of these metals into the ocean, hence we regard the scenario that methanogens be limited by the availability of these metals as less likely than the scenario of H_2-limitation.

Supplementary Figures

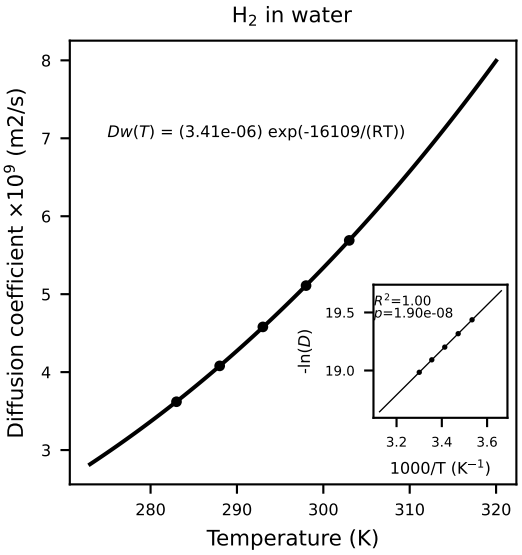

Figure S1 | Diffusion constant of H_2 in water as a function of temperature. Data from ref.[8].

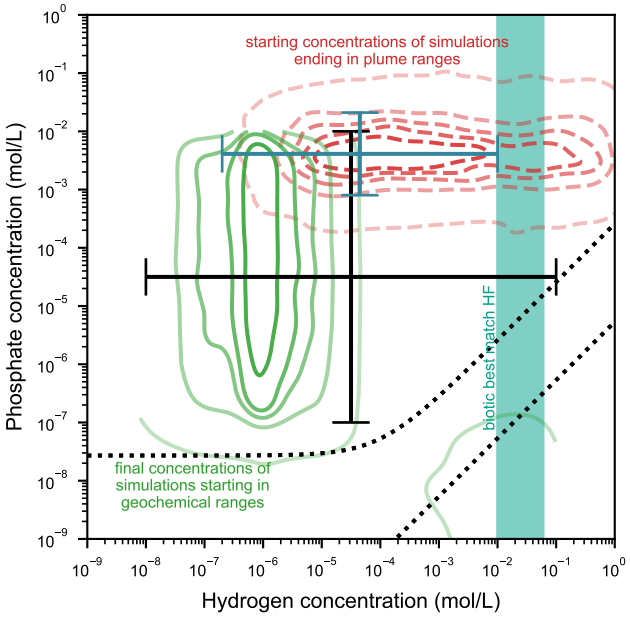

Figure S2 | Resource diagram with biotic initial and final states. Error bars represent ranges of H_2 and P concentrations inferred from chemical analysis of plume material (green) or derived from geochemical calculations (dark), they are the same as in Main Text Fig. 4. The green vertical span highlights the range of H_2 concentrations for the hydrothermal fluid in the model of ref. [14] such that the H_2 and CH_4 fluxes escaping the hydrothermal system after consumption or production by hydrogenotrophic methanogens that best match escape rates in the plume (ref. [15]; *Supplemetary text* section 1.7). The green levels correspond to the density of a sample of 50,000 simulations of the biotic steady-state resulting from initial states (log-)uniformly sampled in the concentration ranges derived from geochemical calculations (dark error bars). The red dashed levels show the density of starting conditions of simulations that have biotic steady-states that best match a 2D log-normal distribution centered on the intersection of the ranges for the inferred ocean composition from plume chemical analysis (green error bars).

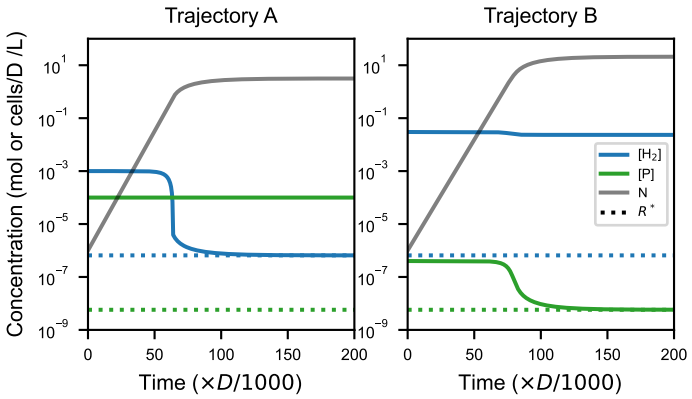

Figure S3 | Trajectories of Main text Fig. 4. as a function of time. Cell density has been rescaled to the dilution rate D, and the time by $D/1000$ for legibility. Solid lines indicate the values of the concentrations of H_2 (blue), P (green) and cells (gray). Dotted lines highlight the values of resource threshold $[H_2]^*$ and $[P]^*$ predicted under our 20-60 °C temperature theoretical scenario (Supplementary Table S1).

Supplementary Tables

Table S1 | Summary of modeling parameterization scenarios.

	T range	0-20 C	20-60 C	60-120 C
	T point	0 C	40 C	80 C
Parameter	Unit			
$v_{max}^{H_2}$	$\mathrm{mol}/(\mathrm{hg_{dw}})$	0.1	1	10
$K_m^{H_2}$	$\mathrm{mol\,L^{-1}}$	5×10^{-6}	2×10^{-5}	6.6×10^{-5}
γ_{H_2}	$\mathrm{mol_{H_2}\,g_{dw}^{-1}}$	2.75	6.6	26.2
v_{max}^{P}	$\mathrm{mol}/(\mathrm{hg_{dw}})$	1×10^{-6}	1×10^{-5}	1×10^{-4}
K_m^{P}	$\mathrm{mol\,L^{-1}}$	1×10^{-8}	2.5×10^{-8}	1×10^{-7}
γ_{P}	$\mathrm{mol_P\,g_{dw}^{-1}}$	1.4×10^{-4}	3.9×10^{-4}	7.1×10^{-4}
$[H_2]^*$	$\mathrm{mol\,L^{-1}}$	2.75×10^{-9}	6.54×10^{-7}	5.6×10^{-6}
$[P]^*$	$\mathrm{mol\,L^{-1}}$	2.81×10^{-11}	5.76×10^{-9}	2.71×10^{-8}

References

[1] Caperon, J. Population growth in micro-organisms limited by food supply. *Ecology* **48**, 715–722 (1967).

[2] Pasciak, W. J. & Gavis, J. Transport limitation of nutrient uptake in phytoplankton 1. *Limnology and Oceanography* **19**, 881–888 (1974).

[3] Klausmeier, C., Litchman, E. & Levin, S. A model of flexible uptake of two essential resources. *Journal of Theoretical Biology* **246**, 278–289 (2007).

[4] Armstrong, R. A. Nutrient uptake rate as a function of cell size and surface transporter density: A michaelis-like approximation to the model of pasciak and gavis. *Deep Sea Research Part I: Oceanographic Research Papers* **55**, 1311–1317 (2008).

[5] Bonachela, J. A., Raghib, M. & Levin, S. A. Dynamic model of flexible phytoplankton nutrient uptake. *Proceedings of the National Academy of Sciences* **108**, 20633–20638 (2011).

[6] Berg, H. C. & Purcell, E. M. Physics of chemoreception. *Biophysical journal* **20**, 193–219 (1977).

[7] Scopes, R. The effect of temperature on enzymes used in diagnostics. *Clinica Chimica Acta* **237**, 17–23 (1995).

[8] Rumble, J. *CRC handbook of chemistry and physics* (CRC press, 2017).

[9] Elias, M., Wieczorek, G., Rosenne, S. & Tawfik, D. S. The universality of enzymatic rate–temperature dependency. *Trends in Biochemical Sciences* **39**, 1–7 (2014).

[10] Affholder, A., Ferrière, R. & Guyot, F. Activation energies of both constructive and destructive cellular biochemistry determine maximum growth temperature in archaea. *Communications Biology* **8** (2025).

[11] Glein, C. R. & Truong, N. Phosphates reveal high ph ocean water on enceladus. *Icarus* **441**, 116717 (2025).

[12] Waite, J. H. *et al.* Cassini finds molecular hydrogen in the Enceladus plume: evidence for hydrothermal processes. *Science* **356**, 155–159 (2017).

[13] Virtanen, P. *et al.* SciPy 1.0: fundamental algorithms for scientific computing in python. *Nature Methods* **17**, 261–272 (2020).

[14] Affholder, A., Guyot, F., Sauterey, B., Ferrière, R. & Mazevet, S. Bayesian analysis of enceladus's plume data to assess methanogenesis. *Nature Astronomy* **5**, 805–814 (2021).

[15] Affholder, A., Guyot, F., Sauterey, B., Ferrière, R. & Mazevet, S. Putative methanogenic biosphere in enceladus's deep ocean: Biomass, productivity, and implications for detection. *The Planetary Science Journal* **3**, 270 (2022).

[16] Higgins, P. M., Chen, W., Glein, C. R., Cockell, C. S. & Sherwood Lollar, B. Quantifying uncertainty in sustainable biomass and production of biotic carbon in enceladus' notional methanogenic biosphere. *Journal of Geophysical Research: Planets* **129** (2024).

[17] Whitman, W. B., Coleman, D. C. & Wiebe, W. J. Prokaryotes: The unseen majority. *Proceedings of the National Academy of Sciences* **95**, 6578–6583 (1998).

[18] Čadek, O. *et al.* Enceladus's internal ocean and ice shell constrained from Cassini gravity, shape, and libration data. *Geophysical Research Letters* **43**, 5653–5660 (2016).

[19] Hao, J. *et al.* Abundant phosphorus expected for possible life in enceladus's ocean. *Proceedings of the National Academy of Sciences* **119**, e2201388119 (2022).

[20] Randolph-Flagg, N. G. *et al.* Phosphate availability and implications for life on ocean worlds. *Nature Communications* **14** (2023).

[21] Postberg, F. *et al.* Detection of phosphates originating from enceladus's ocean. *Nature* **618**, 489–493 (2023).

[22] Xu, W. *et al.* Enough sulfur and iron for potential life make enceladus's ocean fully habitable. *The Astrophysical Journal Letters* **980**, L10 (2025).

[23] Stüeken, E. E. *Biogeochemical nitrogen cycling on the Archean Earth*, 423–432 (Elsevier, 2026). URL `http://dx.doi.org/10.1016/B978-0-323-95547-8.00028-8`.

[24] Cleveland, C. C. & Liptzin, D. C:n:p stoichiometry in soil: is there a "redfield ratio" for the microbial biomass? *Biogeochemistry* **85**, 235–252 (2007).

[25] Affholder, A. *et al.* The viability of glycine fermentation in titan's subsurface ocean. *The Planetary Science Journal* **6**, 86 (2025).

[26] Schönheit, P., Moll, J. & Thauer, R. K. Nickel, cobalt, and molybdenum requirement for growth of methanobacterium thermoautotrophicum. *Archives of Microbiology* **123**, 105–107 (1979).

[27] Thauer, R. K. *et al.* Hydrogenases from methanogenic archaea, nickel, a novel cofactor, and h2 storage. *Annual Review of Biochemistry* **79**, 507–536 (2010).

[28] Lichtenberg, T., Drazkowska, J., Schönbächler, M., Golabek, G. J. & Hands, T. O. Bifurcation of planetary building blocks during solar system formation. *Science* **371**, 365–370 (2021).

[29] Sekine, Y. *et al.* High-temperature water–rock interactions and hydrothermal environments in the chondrite-like core of enceladus. *Nature Communications* **6** (2015).

[30] Yokoyama, T. *et al.* The elemental abundances of ryugu: Assessment of chemical heterogeneities and the nugget effect. *Geochemical Journal* **59**, 45–63 (2025).

[31] Lauretta, D. S. *et al.* Asteroid (101955) bennu in the laboratory: Properties of the sample collected by osiris-rex. *Meteoritics & Planetary Science* **59**, 2453–2486 (2024).

[32] Fisher, T. & Ferriere, R. Potential metabolic viability on asteroid chemistry. *Communications Chemistry* **9** (2026).